Impact of Small Changes in Particle Surface Chemistry for Unentangled Polymer Nanocomposites

Abstract: We report microstructural and rheological consequences of altering silica particle surface chemistry when the particles are suspended in unentangled polyethylene glycol with a molecular weight of 400. The particle surfaces are altered by reacting them with isobutyltrimethyoxysilane. Levels of silanization are chosen so that the particles remain dispersed in the polymer at all volume fractions studied. Our studies indicate that at the levels studied, silanization does not alter the hydrodynamic thickness of the absorbed polymer layer thickness. Rheological properties are not sensitive to levels of silanization up to particle volume fractions where the average particle separation $h \sim 6Rg$ (4.8nm). At these volume fractions, composite microstructure undergoes changes associated with jamming of soft particles (decorrelations in the first peak of the particle structure factor and the onset of a non-diffusive mechanism that dominates particle density fluctuations at short times.) In the region of volume fractions where h/Rg < 6, the zero-shear rate viscosity of the composites is extremely sensitive to level of silanization with a decrease in the zero-shear rate viscosity by four orders of magnitude observed for the highest levels of silanization studied in comparison to the bare particles.

I. INTRODUCTION

Polymer composites are typically composed of inorganic fillers dispersed in a polymeric matrix and have applications in coatings, tires, airplane wings and windmill blades. Composites in which fillers have at least one dimension less than 100 nm are known as nano-composites.[1] Shrinking filler size is associated with enhancements in mechanical, electrical, optical and flow properties.[1-3] The dispersion of these fillers in the polymer is key to optimizing the benefits derived from the small particle size. Particle dispersion is surprisingly difficult and requires enthalpic gains of polymer adsorption to particle surface in order to balance the decreases in entropy associated with how the particle surface alters polymer configuration.[4, 5] At the same time there is evidence that as the particle size shrinks and the strength of attraction between polymer segments and the particle surface diminishes, the mechanical properties of nanocomposites can be dramatically altered.[6-8] Synthesis strategies have been used to modify the surfaces of particles to disperse them in polymer melts. Green et al. explore the consequences of changing the graft density and bulk polymer chain length on the miscibility of PDMS grafted silica particle in PDMS as well as its rheological consequences by using a "graft-to" strategy.[9] Kumar et al. discuss "graft from" strategies that have been developed to achieve high graft densities.[8] These studies however are in the regime where there is no enthalpic interaction between the bulk polymer segments and the grafted surface and the particle dispersion is purely from entropic contributions of bulk / graft polymer interactions. In our study, we alter the surface chemistry in an attempt to modulate the enthalpic interaction term between the polymer segment and the particle surface and explore its effects on the mechanics and microstructure of nanocomposites and where particle volume fraction is driven to a point where particles are separated on the order of the polymer radius of gyration.

Experimental work with silica nanoparticles dispersed in polymer melts have attempted to tune strength of particle-segment interaction strength by changing the polymer chemistry as well as introduction of a co-solvent.[6, 10] Results from these studies were subsequently interpreted using the polymer reference interaction site model (PRISM) and the enthalpy of exchanging a polymer segment form the bulk to the particle surface, ε_{pc}, was measured by comparing PRISM predictions of structural behavior (structure factor at zero angle – S(0)) to experimental data. ε_{pc} is the enthalpic interaction between the polymer segment and the particle surface. PRISM predictions are only weakly dependent on other parameters such as the range of interaction α and degree of polymerization N. Detailed studies by Schweizer and coworkers have established that the phase behavior is primarily controlled by the segment - surface interaction.[4, 5, 11] In the case of hard sphere interactions, $\varepsilon_{pc} = 0$. Entropy - driven depletion flocculation is observed generally where $\varepsilon_{pc} < 0.1 - 0.25$ (weakly depending on other details of the system such as polymer chain length, particle and segment diameter etc). In the range where $0.25 < \varepsilon_{pc} < 2$, the particles are stabilized by the adsorbed segments and are miscible up to high volume fractions. In the range of extremely strong interactions, where typically $\varepsilon_{pc} > 0.8 - 0.9$ at high volume fractions and $\varepsilon_{pc} > 2 - 3$ at low volume fractions, bridging aggregation is observed which results from segments from the same polymer chain sticking to different particles resulting in an aggregate.[4-6, 11] For low molecular weight polymers, the phase behavior of the silica-polymer systems was found to be consistent with PRISM predictions for the measured ε_{pc} values. For polytetrahydrofuran (PTHF), the ε_{pc} value was measured to be 0.35[6] and an onset of aggregation was observed at high volume fractions as well as polymer slip[12] at the particle surface during rheological measurements. For poly(ethylene glycol) (PEG), ε_{pc} was measured as 0.55 and dispersions of particles in the polymer melt were stable at all volume fractions.[6] For low molecular weight PEG, measurements of rheology, NMR nuclear spin relaxation rates, and neutron scattering techniques confirm the presence of an adsorbed layer of polymer. The ε_{pc} values were sensitive to addition of co-solvent such as ethanol or water in the polymer melt and a direct correlation between the ε_{pc} values and the intrinsic viscosity $[\eta]$ was established.[7] PRISM is unable to capture the observed increases the particle effective hydrodynamic size that grows linearly with the polymer radius of gyration[13-15] or the onset of interparticle attractions with increasing polymer molecular weight. The link between hydrodynamic size and suspension structure is not well understood. Thus, PRISM predictions of structure properties are strongly dependent on a single interaction strength parameter ε_{pc} between the polymer segments – particle surface and do not account for any other effects such as the polymer configuration on the surface, thickness of the adsorbed layer or its softness. This is also manifested in the above studies where PRISM calculations of structural quantities such as the structure factor at the first peak are only qualitatively predicted. This is one of the limitations of PRISM which successfully predicts phase behavior but has limitations in predicting the complete structure of the nanoparticle suspensions.

The previous studies above demonstrate the effects of changing polymer particle interactions by altering the polymer chemistry. Here we are interested in investigating the effects of changing polymer-particle interactions by changing the particle surface chemistry. We probe the silica-PEG system using methods such as rheology, static and

dynamic scattering to characterize the changes to nanocomposite properties while changing surface chemistry. We find that the nanocomposite properties diverge in the limit of $h/Rg < 6$ as seen by rheology as well as static and dynamic scattering. From our scattering studies, we also demonstrate that for conditions where the particle-polymer segment interaction strength ε_{pc}, as interpreted within the framework of PRISM, are apparently identical, nanocomposite properties can be profoundly different.

Further, we observe non-monotonic behavior in structural trends that are expected to change monotonically[6] with the particle-polymer segment strength, indicating that there are additional factors than the particle-polymer interaction strength in controlling the microstructure of nanocomposites when the surface chemistry is altered. A detailed understanding into the workings and assumptions of PRISM as applicable to particle-polymer nanocomposites are covered in work by Hall and Anderson[6] as well as Kim et al.[10] For our work, which is an extension of the same silica-PEG system as used in their work, we have utilized the same assumptions as justified by them.

Our model system involves the well-studied system of Stober silica particles suspended in polyethylene glycol (PEG). Rheological studies[13] on these particles in PEG melts indicate that the adsorbed layer creates an effectively larger hydrodynamic size such that composite rheology is that of weakly interacting particles up to high volume fractions. For PEG-400 (PEG with a molecular weight of 400) and particle diameter, $D_c = 44$ nm up to a volume fraction of $\phi_c \sim 0.43$, composite melts respond mechanically like hard spheres suspended in a Newtonian fluid with an effective diameter of $D_H = D_c (1 + 2.9Rg)$ where $Rg = 0.8$nm is the polymer radius of gyration and an effective volume fraction $\phi_{eff} = \phi_c (1 + 2.9Rg/D_c)^3$. These studies indicate that the composite melt displays glassy dynamics when $\phi_{eff} > 0.58$.[16] For PEG-400, this volume fraction is crossed before the average particle surface separation:

$$h = D_c ((\phi_m/\phi_c)^{1/3}-1) \tag{1}$$

is less than $\sim 6Rg$. Here ϕ_m is the maximum packing fraction of the particle cores ($\phi_m = 0.63$).

Studies on higher molecular weight polymers show that when $h/Rg < 6$, the nanocomposite rheology changes dramatically suggesting the effects of polymer confinement are experienced at this average surface separation.[17] Consistent with these mechanical properties is the observation that $1/S(0)$ and $S(q^*D_c)$ pass through maxima at $h \sim 6Rg$. Here $S(0)$ is the zero angle limiting value of the particle structure factor and $S(q^*D_c)$ is the magnitude of the structure factor at the first peak corresponding to the intensity of correlations associated with the first nearest neighbor shell. A maxima in $S(q^*D_c)$ has been associated with a change in pair potential from harsh at large separation to softer at small separations.[18, 19] The microstructural interpretation of the loss of correlations in nearest neighbors with increasing volume fraction lies in some particles being closer together so that other particles experience more free volume and thus experience greater entropy.[18] Srivastava et al. demonstrate a maxima in $S(q^*D_c)$, a hallmark of soft particle behavior, with increasing volume fraction in systems where

polymers are end-grafted to a particle surface.[19] The volume fraction and magnitude of the maxima in $S(q*D_c)$ are dependent on the details of the pair potential.

At low volume fractions, density fluctuations of particles in low molecular weight polymer melts decay in a diffusive manner. This is evidenced in dynamic light and X-ray scattering experiments by density relaxation times decaying as $1/q^2$ where q is the scattering vector.[20, 21] At high volume fractions, however, in soft systems showing a maxima in $S(q*D_c)$, the characteristic density relaxation times decay as $1/q$ indicating ballistic relaxation behavior.[22-27] These observations indicate that there is a transition of relaxations due to self-diffusion out of nearest neighbor cages to alternative relaxation mechanisms such as have been recently discussed by Das et al.[28] Furthermore, the relaxation time of the system shows a non-monotonic trend with respect to the particle volume fraction. This counter-intuitive increase in the speed of density fluctuations decay has been reported previously for water[29-31] and in silica/PEG systems where the polymer is end grafted to the particle surface.[19]

Here we extend studies of the PEG-silica system to cases where surface modified particles are suspended in PEG melts. We alter polymer/particle interactions by reacting the particle surface with isobutyltrimethoxysilane which will replace some of the surface hydroxyl groups with isobutyl groups in increasing amounts and study changes in microstructure, flow and relaxation properties up to high volume fractions. The reaction technique used here is expected to create incomplete silane monolayers on the surface and the coverage is expected to increase monotonically with degree of silanization.[32]

We have chosen to work here with PEG with a molecular weight of 400 that corresponds to a degree of polymerization of 8. This molecular weight was chosen because silica composites at this molecular weight have been well characterized rheologically and structurally.[6, 7, 10] Our studies suggest that at the levels investigated, silanization has a small effect on suspension microstructure and flow properties at the low volume fractions where the composite mechanics are essentially those of particles suspended in a Newtonian fluid and that the particle's hydrodynamic diameter is not impacted by surface treatment. At elevated volume fractions, where $h < 6Rg$, the impact of surface treatment becomes evident with higher levels of surface treatment giving rise to faster relaxation of density fluctuations and lower composite viscosities. These studies suggest polymer dynamics near the particle surface are sensitive to particle surface chemistry where increasing the degree of surface silanization results in more rapid polymer relaxation rates. We expressly probe conditions where bare and silanized particles have similar microstructures. The observed differences in composite dynamics demonstrate a decoupling of dynamics and particle microstructure when absorbed polymer layers are confined.

Below in Section II, we describe our experimental system. In Section III, we present and discuss our results and draw conclusions in Section IV.

II. EXPERIMENTAL

Sample Preparation

Silica particles were synthesized using the method described by Stober et al[33] and the recipe used is more specifically described by Bogush et al[34] The particles were synthesized by the base-catalyzed hydrolysis and condensation of tetra ethyl orthosilicate (TEOS) in ethanol at 55°C. 3610 mL of ethanol was mixed with 96 mL of deionized water and 156 mL of ammonium hydroxide. The mixture was allowed to stabilize to 55°C for 2 hours after which 156 mL of TEOS was added and the reaction was run for 12 hours. Silica particles with diameter D_c = 42±4 nm were obtained at 1.33% w/w in ethanol. The size of the particles was characterized using dynamic light scattering using a 514 nm argon laser. Alternatively fitting the form factor of the particles obtained from X-ray scattering of a dilute suspension with a Gaussian particle size distribution and a standard deviation of 10% gave the same result. The silica suspension in ethanol was concentrated slowly to ~17% wt by slow evaporation at 60°C in a solvent hood.

Other identical batch of silica particles were synthesized and characterized but these batches of particles were reacted with varying degrees of isobutyltrimethoxysilane. We report the amount of silane used as a weight percent of silane added based on the mass of silica in the suspension. Up to 5 wt% silane based on the mass of the silica was added to the suspensions to create surface-treated particles rendered partially hydrophobic due to replacement of surface hydroxyl groups with isobutyl groups. This was carried out by first concentrating the batch to approximately 4.5% of silica by weight and then adding a 1% ethanolic solution of the silane drop-wise over a course of 10 minutes at a temperature of 70°C. The quantity of the silane solution was determined based on the degree of silanization desired (0-5% w/w on silica). The reaction was then kept at 70°C for 3 hours. After this the batch was then concentrated to ~17% wt similar to the bare silica particles.

The anhydrous reaction conditions chosen for silanization of the particles typically give monomeric coverage of the particles instead of the deposition of oligomeric siloxane layers that tend to make the surface coverage patchy.[32] Monolayers of silane are typically of the order of 6-10 Å ($<< D_c$).[35] This ensures that the silane coverage on the particle does not alter the particle diameter in any significant manner. This is supported by DLS and x-ray scattering measurements that show no difference in diameter between the bare and silanized particles. Assuming the particle diameter of 42 nm, a surface area of 89 m^2/g is calculated, given particle density of 1.6 g/m^2. The specific coverage area of isobutyltrimethoxysilane is ~ 450 m^2/g (Gelest® Product Catalog) giving a surface coverage of 20% at 5% silanization.

Polyethylene glycol with a molecular weight of 400, PEG-400 was purchased from Sigma Aldrich®. The radius of gyration, Rg, of PEG-400 is ~ 0.8 nm and is composed of 9 ethylene glycol units[13]. The segment diameter is 1.6 nm.[7] The viscosity of PEG-400 was measured to be 1.6x10^{-2} Pa.s at 75°C and 9.3x10^{-2} Pa.s at 25°C.

Concentrated silica suspensions were then added in the needed amount to the PEG-400 in a 20 mL scintillation vial. The mixture was then thoroughly mixed using a vortex mixer. The final composite samples were prepared by driving off the ethanol in a vacuum oven at 90°C after purging with nitrogen several times to ensure that oxygen does not degrade the polymer. The silica concentrations in PEG were prepared at pre-determined weight fractions due to higher accuracy measuring weight rather than volume. The volume fraction of the silica particles is subsequently calculated by using density of silica particles[13] ρ_c as 1.6 g/cm^3 and that of PEG-400 ρ_p is 1.13 g/cm^3. Thus, the formula for ϕ_c is:

$$\phi_c = \frac{\rho_p}{\rho_c}\left(\frac{m_c}{m_c+m_p}\right) \tag{2}$$

During sample preparation, the final samples spontaneously cracked as the volume fraction was increased beyond a critical value. For the bare samples, the first signs of cracking were seen at volume fraction of $\phi_c = 0.51$ and above, whereas the silanized samples showed cracking at $\phi_c > 0.55$. The cured silica-PEG system can be viewed as silica particles with an immobile polymer layer adsorbed at the surface and dispersed in a sea of free polymer. As the volume fraction is increased and the average particle separation decreases, the fraction of free polymer in the system drops and becomes small compared to adsorbed polymer. At some point, there is not enough free polymer to fill the spaces in between the particles, but the particles and their absorbed layers are not able to come in close enough for the adsorbed layer to fill these spaces. Thus, at elevated volume fraction the system develops internal stresses associated with desaturation of the particle resulting in fracture of bulk samples that transition from tractable, flowable to brittle and crumbly. For a system of bare silica particles dispersed in PEG-400, we expect a diameter increase for the particles of $2.9Rg$[13] to give an effective volume fraction of the particles $\phi_{eff} = \phi_c[1 + 2.9Rg/D_c]^3$. Therefore, it is expected that at $\phi_{eff} \sim 0.63$ (the hard-sphere maximum packing volume fraction) or, for our system at $\phi_c \sim 0.53$, the particles and strongly absorbed polymer layers are in surface to surface contact with each other and a desaturation of free polymer should occur at higher volume fractions. Thus, the volume fraction at which we begin to see cracking in the bare system is approximately in line with our expectations. Of particular interest is the consistent and repeatable difference in volume fraction where cracks first form, with the silanized samples always remaining crack free to larger volume fractions than the bare samples and thus indicating greater capacity to accommodate decreased volume of unbound polymer.

Rheology

The zero shear rate viscosities of the sample were measured using a TA instruments DHR-3 torque controlled rheometer. Cone and plate geometry using a 20 mm 4° cone was used with a gap size of 112 microns. All measurements were carried out at 75 °C in order to ease handling of extremely viscous samples at volume fractions above 0.40.

Static Scattering (SAXS)

The small angle X-ray scattering (SAXS) studies on the samples were carried out at Advanced Photo Source (Argonne National Lab) at 12-ID-B and 5-ID-D. Measurements at 12-ID-B were carried out using Pilatus 2M detector, sound-bounce monochromator and a beam energy range of 7.9-14 KeV. At 5-ID-D, a Si(111) type monochromator and a beam energy range of 6.5-17 KeV was used. 1 mm borosilicate glass capillaries from Charles Supper$^{®}$ were used. For samples above the colloidal glass volume fraction, the polymer-particle-ethanol mixture was used to form a film in a custom made aluminum slide with a single 3 mm hole with 0.5 mm depth in which a film of silica / PEG / ethanol was formed and then dried in a vacuum oven under the same conditions and duration as the samples cured in the vials.

Dynamic scattering studies on the samples were done at Advanced Photon Source (Argonne National Lab) using X-ray photon correlation spectroscopy (XPCS) at 8-ID-I using a Dalsa 1M60 CCD Detector. The sample holders were custom-made aluminum slides with a single 3 mm hole of 0.5 mm depth in the middle over which a film of the composite was formed and cured similar to SAXS. The studies were performed at 75°C similar to the viscosity measurements.

The scattering in the silica-PEG composite after subtracting the polymer scattering is considered to only arise from the silica particles thereby justifying the use of an effective one component system.[13] The scattering intensity function $I(q,\phi_c)$ for a one component system is as follows:

$$I(q,\phi_c) = \phi_c V_c \Delta\rho_e{}^2 \, P(q) \, S(q,\phi_c) + B \qquad (3)$$

where q is the wave vector, ϕ_c is volume fraction, V_c is the particle volume, $\Delta\rho_e$ is the net electron scattering length density of the particles compared to the polymer, $P(q)$ is the particle form factor, $S(q,\phi_c)$ is the particle structure factor and B is the background scattering intensity.

The particle form factor is measured in the zero concentration or dilute limit ($\phi_c \rightarrow 0$) where no particle pair correlations exist and therefore $S(q, \phi_{c\rightarrow0}) \rightarrow 1$. Thus the particle structure factor can be measured by dividing the intensity at a given volume fraction by the intensity in the dilute limit while normalizing for the particle volume fractions:

$$S(q,\phi_c) = \frac{I(q,\phi_c)}{I(q,\phi_{c\rightarrow0})} \, \frac{\phi_{c\rightarrow0}}{\phi_c} \qquad (4)$$

Dynamic Scattering (XPCS)

When performing x-ray photoelectron spectroscopy (XPCS), the intensity auto-correlation function $g_2(q,t)$ is measured and is defined as[20]:

$$g_2(q,t) = \frac{<I(q,t')\,I(q,t'+t)>}{<I(q,t')>^2} \;\; ; \;\; t > 0 \qquad (5)$$

The intensity auto-correlation function $g_2(q,t)$ is then modeled approximately with a stretched exponential form of[26]:

$$g_2(q,t) = 1 + b{f_q}^2 \exp[-2\left(\frac{t}{\Gamma}\right)^{\beta}] \qquad (6)$$

where b is the Seigert factor dependent on the instrument measured to be ~ 0.36 in our case, f_q is the non-ergodicity parameter that is a measure of the short time plateau value, Γ is the characteristic relaxation time of the sample, and β is the stretching exponential that characterizes the shape of the relaxation curve.

III. RESULTS AND DISCUSSION

Rheology

In the dilute limit, the zero-shear relative viscosity, $\eta_{r,0}$, increases as:

$$\eta_{r,0} = 1 + [\eta] \, \phi_c \qquad (7)$$

where $[\eta] = 2.5$ in the case of hard spheres experiencing no slip boundary conditions.[36] In case of silica particles in PEG-400, $[\eta] > 2.5$ indicating the presence of an adsorbed immobile polymer layer making the particles seem bigger on an average. Effective hard sphere diameters larger than those of the core for the silica/PEG system have been reported previously by Anderson et al[13], Jiang et al[37] and Kim et al.[7] The values of $[\eta]$ do not vary systematically with silanization indicating that, within the limits of experimental uncertainty the thickness of the adsorbed layer does is not affected in the dilute limit (Fig 1. And Table 1).   An intrinsic viscosity of 2.7 ± 0.2 corresponds to an effective hydrodynamic diameter $D_{eff} = D_c ([2.7\pm0.2]/2.5)^{1/3} = D_c (1.03\pm0.03)$ which is within the expected range predicted by Anderson where a diameter increase of $2.9Rg$ would result in a 5% increase in particle diameter. [17] The results in Table 1. indicate that the polymer adsorbed to the particle surface responds hydrodynamically in a manner that, within the sensitivity of measurement of $[\eta]$, is independent of the level of silanization.
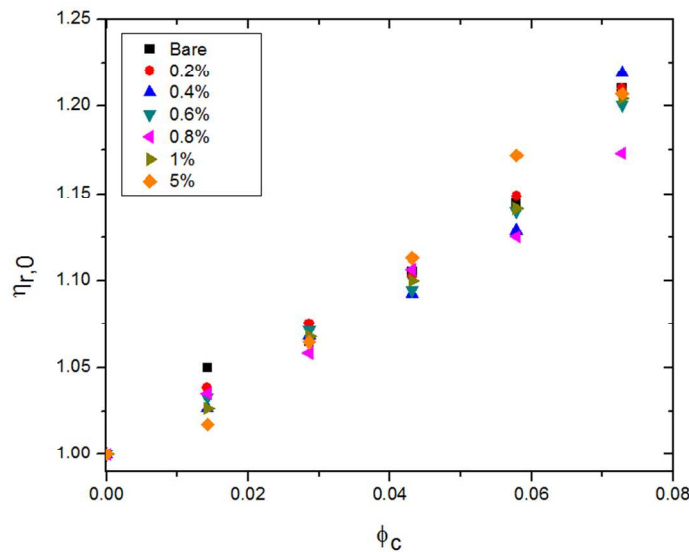

Fig 1. Relative viscosity $\eta_{r,0}$ versus volume fraction ϕ_c for different levels of silanization in the linear region. Silanization percentage is w/w on silica.

Level of Silanization (% w/w on silica)	Intrinsic Viscosity $[\eta]$
0 % (Bare)	2.7 ± 0.2
0.20%	2.8 ± 0.1
0.40%	2.8 ± 0.3
0.60%	2.6 ± 0.2
0.80%	2.3 ± 0.1
1%	2.8 ± 0.2
5%	3.0 ± 0.3

Table 1. Intrinsic viscosities at different levels of silanization % w/w on silica.

As expected from particles of the same effective core diameters (as measured from intrinsic viscosity), at elevated volume fraction, the zero shear rate viscosity is unaffected by levels of silanization for $\phi_c < 0.43$ (Fig.2a). Above this volume fraction, there is a systematic separation of zero shear rate viscosities. For volume fractions up to 0.43 we suggest stress transfer is dominated by hydrodynamic interactions between effective hard spheres with volume fraction of ϕ_c ($[\eta]/2.5$). Also shown in Fig 2a. is the prediction of the Krieger-Dougherty equation[38], $\eta_{r,0} = (1 - \phi_c / \phi_m)^{-2}$ where ϕ_m was chosen to be 0.53 as $\phi_{eff} \sim 0.63$ at this volume fraction. It can be seen that the hard sphere prediction fits well at lower volume fractions but begins to diverge at higher volume fractions. A ϕ_m of 0.48 was found to fit the data much better at higher volume fractions indicating that the particles are larger at higher volume fractions than measured from intrinsic viscosity measurements. It must also be noted that at higher volume fractions the adsorbed polymer layers begin to interact leading to additional repulsion and the system is no longer hard sphere like.

At $\phi_c = 0.43$, h/Rg is approximately 6. For entangled polymers (MW > 2000), Anderson reports rheological anomalies occur for $h/Rg \leq 6$[17] and attributes this to interactions between polymer layers and the disturbance that these adsorbed layers make to adjacent polymer. Under these conditions, the viscosity begins to be dominated by the characteristics of the adsorbed polymer.[17, 37] As shown in Fig 2b., the viscosity in this region shows a monotonic reduction with increasing silanization, suggesting faster relaxation of the adsorbed polymer layer with increasing silanization. In previous work, the adsorbed layer interactions were shown to influence the rheology for $h/Rg < 6$ in entangled systems.[17] Our study shows that onset of these interactions are a universal behavior irrespective of entanglement since our system is unentangled.

In Fig 2c., the viscosity, η, is plotted versus the shear rate, $\dot{\gamma}$, for a fixed volume fraction $\phi_c = 0.49$ ($\phi_{eff} = 0.58$) for different levels of silanization. At the same volume fraction, 5% silanization results in a lowering of the limiting zero shear rate composite viscosity by

approximately 4 orders of magnitude. A drop in viscosity with increasing softness has been reported for particles interacting with soft potentials.[39, 40]
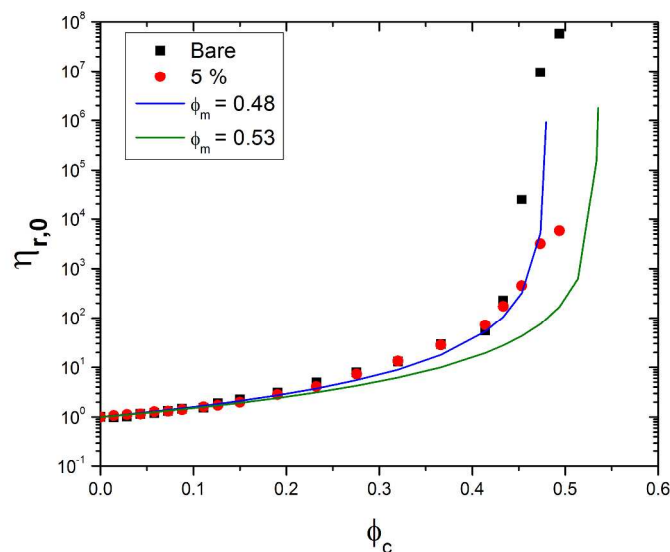

Fig 2a. Zero-shear rate relative viscosity $\eta_{r,0}$ versus volume fraction ϕ_c for bare and 5% w/w silica particles in PEG-400. The zero-shear rate viscosity increases rapidly for the bare particles as the suspension relaxation time drops rapidly at a volume fraction ϕ_c near 0.43 indicating the onset of glassy dynamics. The solid lines indicates the hard sphere viscosity prediction at $\phi_m = 0.48$ and 0.53.
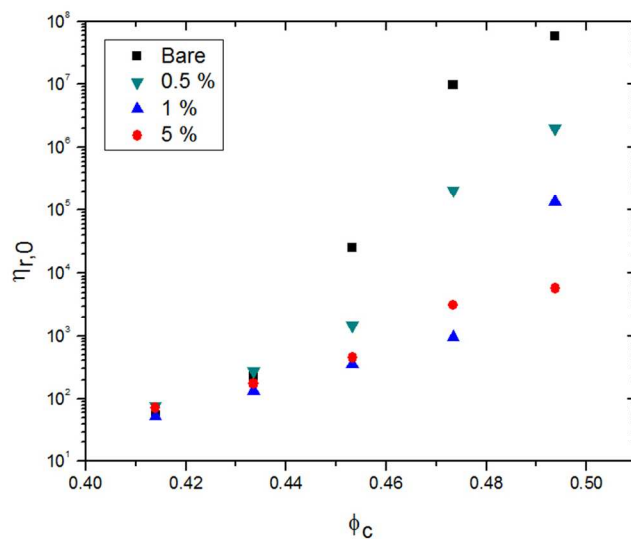
Fig 2b. Relative viscosity $\eta_{r,0}$ versus volume fraction ϕ_c in the high volume fraction regime comparing different levels of silanization % w/w on silica.
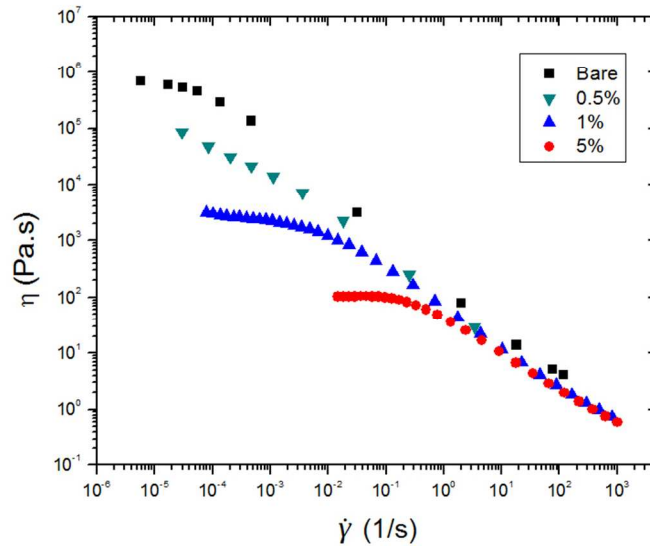
Fig 2c. Viscosity η versus shear rate $\dot{\gamma}$ at $\phi_c = 0.49$ for different levels of silanization.

In Fig 3. we present flow curves of stress (τ) as a function of shear rate ($\dot{\gamma}$) for the bare particles in the high volume fraction region. At low shear rates, the terminal region is reached where the slope ~ 1. At increased shear there is a cross over to a shear-thinning region. The cross over shear rate ($\dot{\gamma}_x$) is a measure of the samples relaxation rate. As the volume fraction approaches a certain cross over value ϕ_x, the shear rate drops rapidly and the slope in the yield stress plateau region decreases rapidly with increasing volume fraction. The slopes in this shear thinning plateau regime ($p = \text{dlog}_{10}(\tau)/\text{dlog}_{10}(\dot{\gamma})$) as a function of ϕ_c for bare particles are listed in Table 2.

Jiang et al[41] defined a cross over volume fraction ϕ_x indicating the onset of glassy dynamics as the volume fraction where the value of $p = 0.5$. The value of p was found to follow a universal behavior when plotted as a function of ϕ_c / ϕ_x. For the systems studied by us, this occurs at $\phi_x \sim 0.43$ or $\phi_{xeff} = 0.43 \, (1+2.9Rg/42)^3 = 0.51$. Jiang found that for hard spheres, $\phi_x = 0.511$, which is in agreement with the samples studied here.
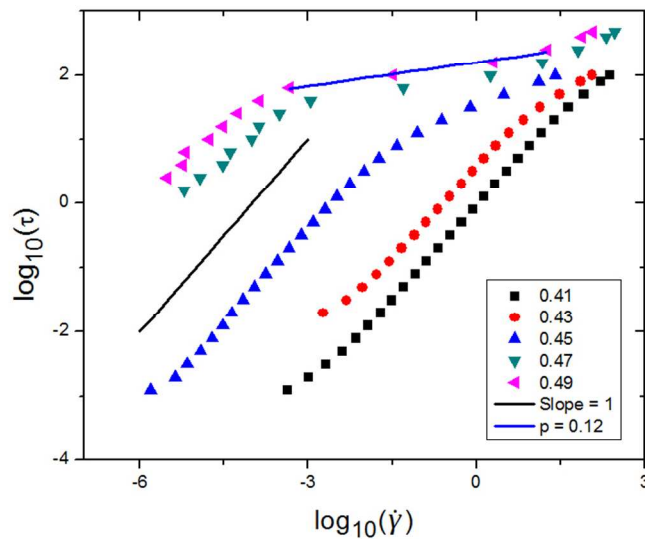
Fig 3. $\log_{10}$-$\log_{10}$ plot of stress τ versus shear rate $\dot{\gamma}$ for bare silica in PEG-400 at various volume fraction ϕ_c. A guideline with a slope of 1 has been provided to compare the low shear terminal regime with. A slope showing the slope of the shear thinning plateau for $\phi_c = 0.49$ has been shown as well.

The p values for the bare and 5% silanized particles in PEG-400 are plotted versus ϕ_c / ϕ_x in Fig 4. Also shown is data from Jiang et al.[41] where R represents the volume fraction of large particles ($D_c = 612$ nm) in a binary mixture with small particles ($D_c = 127$ nm). In the shear thinning region, the curve for the bare particles fit well onto the universal behavior suggesting that up to the colloidal glass transition, bare and silanized particles have similar shear thinning characteristics. For larger volume fractions, the bare and 5% silanized particles diverge. As with the zero shear rate viscosity, when $h/Rg < 6$, the silanized suspensions display a weaker shear thinning response suggesting stress transfer is dominated by alternative mechanisms than seen in the bare particles. The curve for the bare particles drops below that of the universal behavior for $\phi_c / \phi_x > 1$. This is likely due to different methods used to estimate p. For our study, we estimated p by choosing the minimum in $d\log_{10}(\tau)/d\log_{10}(\dot{\gamma})$ as a function of $\log_{10}(\dot{\gamma})$ rather than reporting the average slope over a range of values.

These results suggest that while the particles experience localization at similar volume fractions due to adsorbed layers of approximately the same thickness, as the volume fraction is increased to a point where $h/Rg < 6$ the composite melt flow properties reflect the amount of silane reacted to the particle surface.
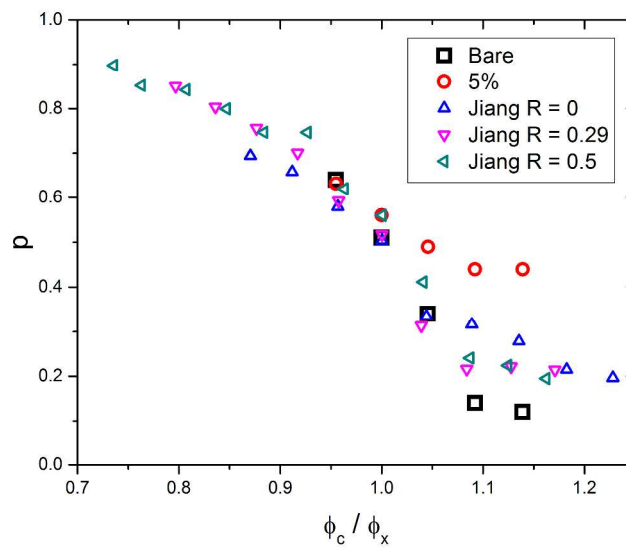
Fig 4. Shear thinning plateau slope p versus normalized volume fraction ϕ_c / ϕ_x for bare and 5% silanized silica particles in PEG-400. Also shown is data from Jiang et al.[41] where R represents the volume fraction of large particles (D_c = 612 nm) in a binary mixture with small particles (D_c = 127 nm).

Structure

In Fig. 5a and 5b., the structure factor $S(qD_c)$ is plotted as a function of qD_c for bare and 5% silanized particles at various ϕ_c. No upturn in $S(q)$ at low q is seen indicating that aggregates are not formed. The structure factors are similar at low volume fractions as shown in the inset in Fig 5b. The first peak in $S(qD_c)$ for the 5% silanized particle composites show slight shifts to higher qD_c at moderate volume fractions compared to the bare. At high volume fractions near $\phi_c = 0.55$, there is downturn in the height of the first peak for both systems, with the bare system showing the larger drop (comparison shown in Fig 5b. inset).

The height of the first peak $S(q*D_c)$ is given as a function of ϕ_c in Fig 6a. Also plotted are PRISM predictions for various values of the interaction strength parameter ε_{pc}. Upon silanization of the particles at 0.2% and 0.4% levels, the curves show an initial decrease in the slope before recovering back up to that of bare particles. Within the PRISM framework, this would be interpreted as a decrease and subsequent recovery in the particle-segment interaction strength. The $S(q*D_c)$ values are plotted for an extended range of ϕ_c through the colloidal glass transition for the bare and 5% silanized particles in Fig 6b.

The $S(q*D_c)$ in Fig 6b. shows a maximum around $\phi_c = 0.45$. The downturn in $S(q*)$ is similar to anomalous structure behavior of soft-core particles as shown by Srivastava et al[19] and Anderson et al.[17] The loss of interparticle correlation and structure near the

jamming transition for soft particles has been discussed in the literature and is associated with average particle spacings that probe two different regimes of softness in pair potential – harsh or stiff at large separations and softer at smaller separations.[18, 42-45]

The bare particles show a maximum in $S(q*D_c)$ at $\phi_c \sim 0.45$, again where h/Rg is slightly below 6 (at 5.24) indicating that the soft repulsions begin approximately where the adsorbed layers are expected to begin interacting. We conclude that for $h/Rg < 6$, the system minimizes free energy through a variation in average particle spacing that results in decorrelation of the first nearest neighbor distance.
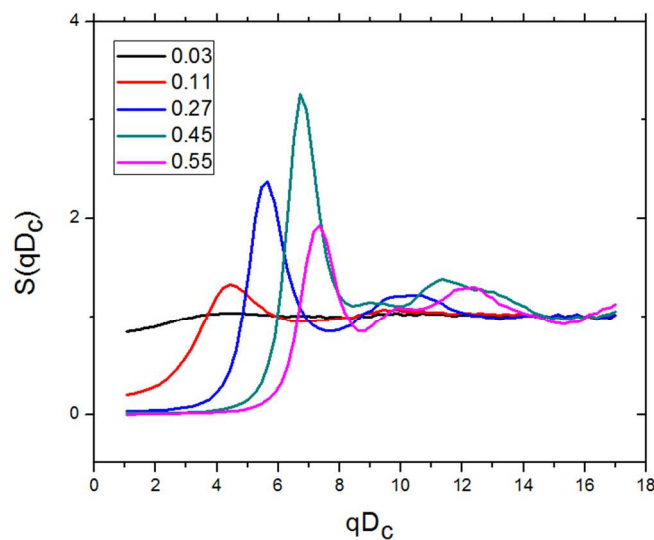

Fig 5a. Structure factor $S(qD_c)$ versus qD_c the wave vector for bare particles that has been non-dimensionalized by the particle diameter (42 nm) for the listed volume fractions ϕ_c.
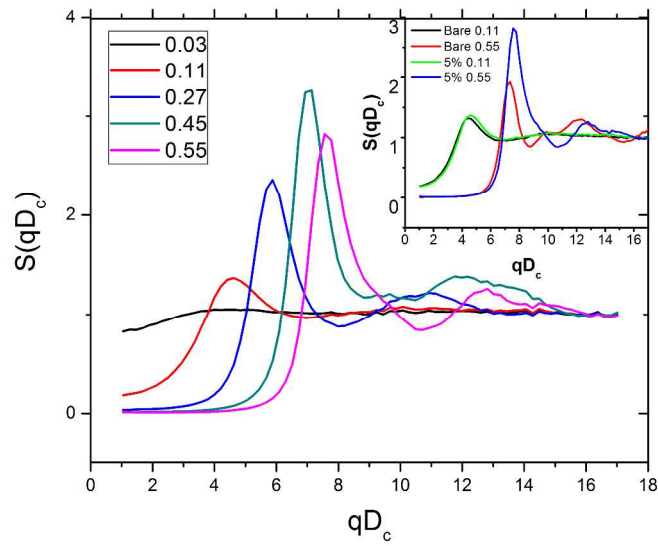
Fig 5b. Structure factor $S(qD_c)$ versus qD_c the wave vector for 5% silanized particles that has been non-dimensionalized by the particle diameter (42 nm) for the listed volume fractions ϕ_c. Additionally, a comparison of bare and silanized structure factors at low ($\phi_c = 0.11$) and high ($\phi_c = 0.55$) volume fractions is shown in the inset indicating the similarity in structures at low volume fraction and the greater loss of correlations in first nearest neighbor spacing for the are particles at $\phi_c = 0.55$.
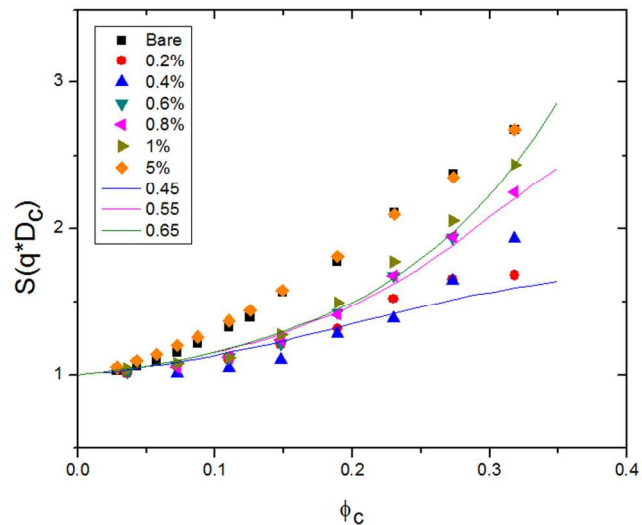

Fig 6a. Height of the first peak $S(q^*D_c)$ versus volume fraction ϕ_c for different levels of silanization. Also shown are PRISM predictions for ε_{pc} values of 0.45, 0.55 and 0.65 showing increasing slopes.
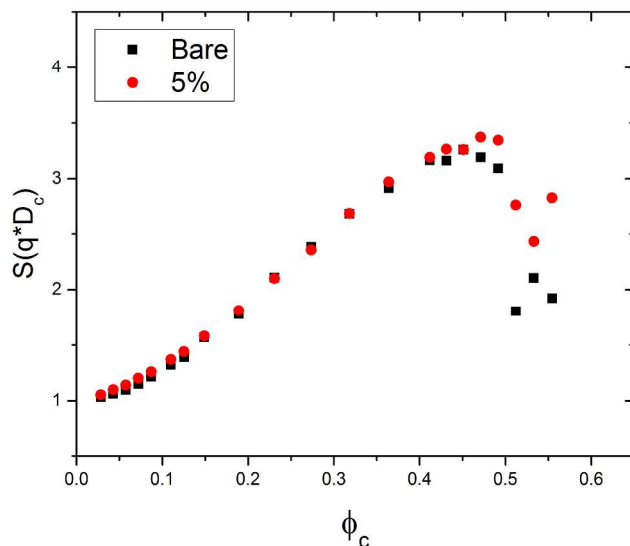
Fig 6b. Structure first peak height $S(q*D_c)$ versus volume fraction ϕ_c for an extended range of volume fraction through the colloidal glass transition for bare and 5% silanized silica in PEG-400.

Fig 7a. shows a non-monotonic trend in the change of the inverse osmotic compressibility $1/S(0)$ ($1/S$ in the limit $qD_c \rightarrow 0$) when plotted versus ϕ_c. Similar to what is observed with $S(q*D_c)$, there is an initial drop in $1/S(0)$ for the 0.1% silanized samples followed by a recovery with increasing silanization. Interpreted through the framework of PRISM, this would indicate a decrease in the particle-polymer interaction strength, followed by a subsequent recovery similar to trends seen in $S(q*D_c)$. The non-monotonic trends seen here indicate that the structural behavior is not captured by a variation of the interaction strength parameter alone and point to other additional factors that are not captured by the PRISM model. A possible explanation may involve configurational changes in the adsorbed polymer layers that reflect in the recovery of structure at higher silanization levels leading to non-monotonicity.

A comparison of the bare and 5% silanized particles over a wider range of volume fractions are given plotted in Figure 7b. Previous work by Anderson et al[6] and Kim et al.[7, 10] with the same system has been shown to overlay up to high volume fractions with a PRISM curve of $\varepsilon_{pc} = 0.55$, which is approximately seen for our bare and silanized particles as well. This along with similar intrinsic viscosity results gives us confidence in extending their work in the direction of surface treatment. There is a sharp maximum in $1/S(0)$ around $\phi_c \sim 0.45$ for both silanized and bare particles. The bare particle composites recover to a trend of increasing $1/S(0)$ over a small change in ϕ_c while the silanized particles show suppressed values over a broader range of volume fraction range. We note that the maximum for both systems occurs where $h \sim 6Rg$. For $0.45 < \phi_c < 0.52$, long wave length density fluctuations are easier to produce in the silanized system (i.e., the 5% silanized system is more compressible compared to the bare). At $\phi_c \sim 0.52$ where $h/Rg \sim$

3, increasing volume fraction results in lower compressibility. As shown in previous work by Anderson et al[17] and Granick and co-workers,[46, 47] at this separation distance, particle surfaces experience a strongly repulsive interaction. This result is consistent with a regime where the glassy nature of the polymer segments near the particle surface and hard silica cores become important resulting in less compressibility at $h/Rg \leq 3$.

Thus, these results are consistent with particles that experience a harsh repulsion for separations larger than $6Rg$ and they experience a change in potential of mean force when $h/Rg \leq 6$ followed by reversion back to harsh repulsions at $h/Rg \leq 3$.
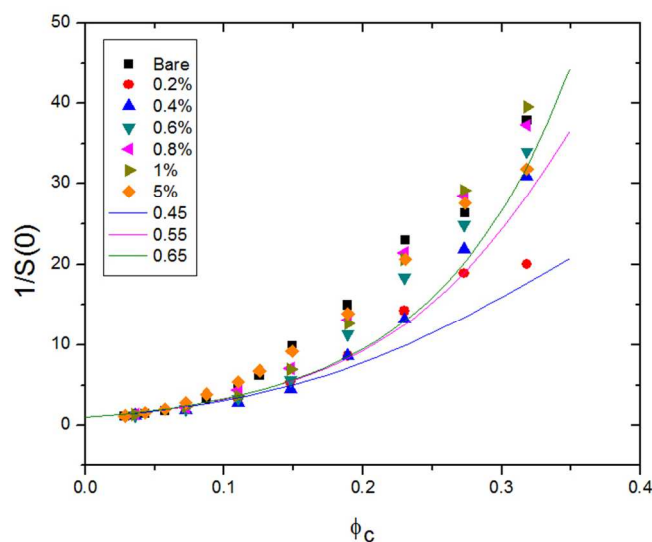

Fig 7a. Inverse osmotic compressibility $1/S(0)$ versus volume fraction ϕ_c for different levels of silanization % w/w on silica. Also shown are PRISM predictions for $\varepsilon_{pc} = 0.45$, 0.55 and 0.65 showing increasing slopes.
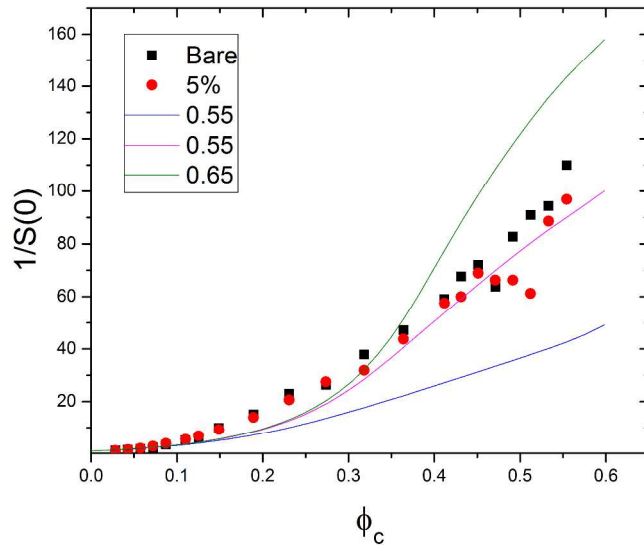
Fig 7b. Inverse osmotic compressibility $1/S(0)$ versus volume fraction ϕ_c for bare and 5% silanization w/w on silica. PRISM predictions for ε_{pc} = 0.45, 0.55 and 0.65 are also shown.

Dynamic Scattering / Density Relaxations

On the basis of zero shear rate viscosities, we expect the silanized particles to display more rapid density fluctuations than observed with bare particles when $h/Rg < 6$. To test this hypothesis, intensity auto-correlation experiments were undertaken for the bare and 5% silanized particles in PEG-400 in the high volume fraction regime. The dynamic correlation functions were measured only for samples of ϕ_c = 0.47 and above as the samples below this volume fraction decayed too rapidly to capture the short time plateau value using the fastest detector. We note that this is well into the volume fraction regime where we expect the particles to display glassy dynamics ($\phi_c>0.43$)

An illustrative example of the intensity auto-correlation function $g_2(q*,t)$ as a function of delay time t is shown for two volume fractions for bare and 5% silanized samples in Fig 8. The curves are fit to the equation of the form:

$$g_2(q,t) = 1 + bf_q{}^2\exp[-2\left(\tfrac{t}{\Gamma}\right)^{\beta}] \qquad (8)$$

where b is the Seigert factor dependent on the instrument measured to be $\sim$ 0.36, f_q is the non-ergodicity parameter that is a measure of the short time plateau value, Γ is the characteristic relaxation time of the sample, and β is the stretching exponential that characterizes the shape of the relaxation curve.[26]
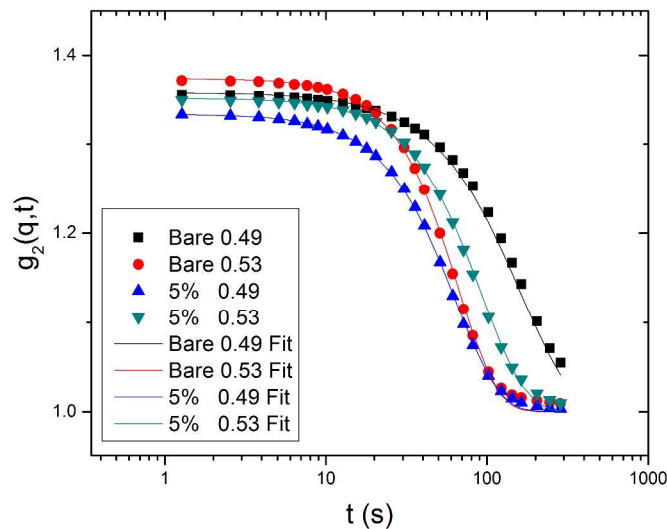
Fig 8. Intensity auto-correlation function $g_2(q,t)$ as a function of delay time t for bare and 5% silanized particles at different volume fractions at q^*. Also shown are fits to equation 8.

From the fit, we are able to extract values of Γ and β for all the samples at q^*. The values are listed in Table 3. The characteristic relaxation time Γ and wave vector q are plotted in Fig 9 in the form of $\log_{10}(\Gamma)$ as a function of $\log_{10}(q)$

Bare				
q^* (Å^{-1})	ϕ_c	Γ (s)	$\beta \pm 0.2$	f_q
0.0162	0.47	279	1.61	0.88
0.0162	0.49	258	1.41	0.98
0.0177	0.51	118	1.62	0.99
0.0177	0.53	92	1.57	0.99
5% Silanized				
q^* (Å^{-1})	ϕ_c	Γ (s)	$\beta \pm 0.2$	f_q
0.0184	0.47	65	1.57	0.91
0.0184	0.49	92	1.68	0.94
0.0184	0.53	128	1.72	0.97
0.0184	0.56	153	1.72	0.99

Table 3. Values of the position of the first peak q^*, volume fraction ϕ_c, characteristic relaxation time Γ, the stretching exponential β, and short time plateau measure f_q for the bare and 5% silanized samples.

There are two features of importance in the g_2 curves. First, $f_q \sim 1$ for bare and silanized samples. These results suggest that we are able to capture the fastest characteristic relaxation process of the bare and silanized samples. Second, moving from $\phi_c = 0.49$ to 0.53 results in an increase in Γ for the silanized indicating that density fluctuations relax more slowly with increasing volume fraction. However Γ decreases for the bare particles such that density fluctuations relax more rapidly.
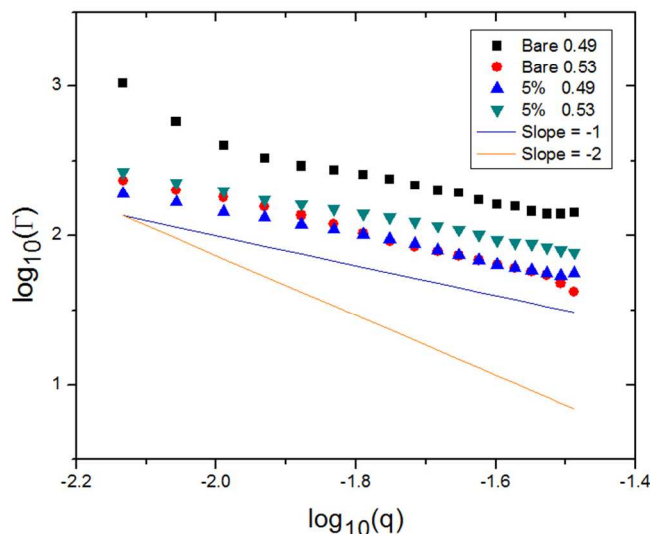

Fig 9. $\log_{10}$-$\log_{10}$ plot of characteristic relaxation time Γ versus wave vector q. Guide-lines with slope of -1 and -2 are plotted for the sake of comparison.

As can be seen from Table 3, the values of $\beta > 1$ which implies a compressed exponential relaxation time. As noted by Guo et al., compressed exponential type decay has been widely reported[22-24, 26, 48-51] and is a signature of hyper-diffusive motion that has been observed in colloidal gels and systems comprising of soft particles.

The characteristic relaxation time Γ is plotted as a function of wave vector q in Fig 9. As can be seen the relaxation time Γ scales as $1/q$ instead of $1/q^2$ indicating that the particles are subject to ballistic rather than diffusive motion. This ballistic relaxation occurs at all volume fractions studied here for both bare and silanized particles This non-diffusive scaling phenomenon has been widely reported for jammed soft systems and glassy liquids.[22-27, 48-54] It has also been seen specifically in silica-PEG systems.[19]

The characteristic relaxation time Γ at q^* is plotted as a function of volume fraction ϕ_c for both the bare and silanized systems in Fig 10. It can be seen that there is a decrease in Γ with volume fraction for the bare particles. This counter-intuitive speed up of relaxation times has been reported in previous work with similar systems, silica particles with endgrafted-PEG in PEG melts, and in general, this increase in velocity is seen in systems with primarily soft-core interactions.[19]

Fig 10. shows that unlike the bare particles, the silanized particles display a monotonic increase in Γ with increasing volume fraction. We observed that the decrease in Γ for the bare particles was associated with the onset of cracking in the samples at $\phi_c > 0.49$ whereas the 5% silanized samples did not show cracking till $\phi_c > 0.55$. We speculate that the 5% silanized samples too would have shown a downturn beyond $\phi_c > 0.55$ where cracking is observed. Unfortunately, those samples could not be loaded onto the instrument due to their stiffness. Cracking is associated with desaturation of the particle bed (i.e., there is not sufficient unbound polymer to fill the spaces between the particles). Silanization delays the desaturation to higher volume fractions suggesting that the particles are able to move closer before desaturation occurs indicating greater adsorbed polymer mobility or increased softness in keeping with the greater density relaxation rates initially. The link between onset of cracking and the downturn in Γ is possibly fortuitous and whether they are inherently linked is open to investigation.
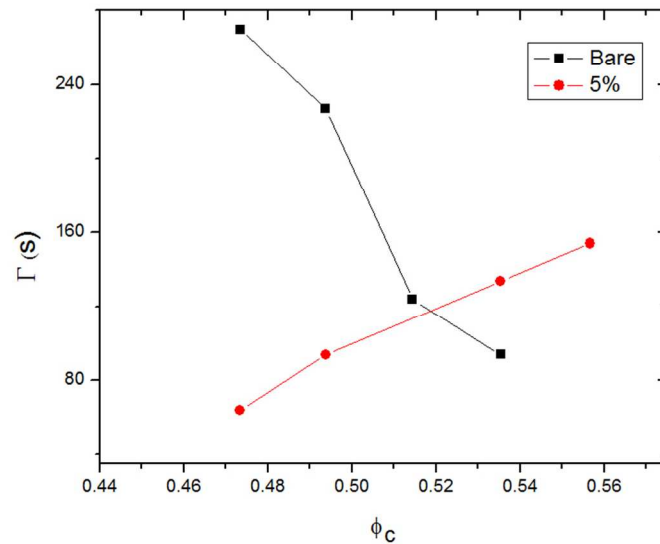

Figure 10. Characteristic relaxation time Γ versus volume fraction ϕ_c for bare and 5% silanized particles in PEG-400.

We compare the values of Γ for the bare and 5% silanized samples at ϕ_c of 0.49 with a characteristic relaxation time extracted from rheological measurements (Fig 2c.) Γ_r defined as the inverse of the shear rate where $\eta=0.9\eta_0$, and is taken as a surrogate for a characteristic diffusion time for the particles. For $\dot{\gamma}\,\Gamma_r \ll 1$ the particles are in equilibrium and shear does not alter microstructure. For $\dot{\gamma}\Gamma_r > 1$, the shear deforms the composite faster than diffusion can relax the induced structural changes and the system shear thins. As can be seen in Table 4, Γ_r increases rapidly with increasing volume fraction for the bare particles while the increase is not so dramatic for the silanized particles indicating greater mobility as probed by steady shear. On the other hand, there is no correlation between Γ_r and Γ measured by dynamic X-ray scattering. At rest, density relaxations occur via processes that are de-correlated from those that control the onset of shear thinning. The onset of shear thinning in colloidal systems at high volume

fractions is associated with relaxation mechanism involving the transport of the particles outside of their nearest neighbor shell. Near the glass transition, this becomes increasingly difficult resulting in very large changes in the relaxation time over a small range of volume fraction. The fact that the relaxation times from XPCS are minimally affected in this range indicates that the relaxation mechanism probed by XPCS likely involves a relaxation mechanism of a different origin. This is supported by the observation that Γ scales as $1/q$ instead of $1/q^2$ that is associated with diffusive motion.

ϕ_c	Bare		5% Silanized	
	Γ_r (s)	Γ (s)	Γ_r (s)	Γ (s)
0.45	821	N/A	0.4	N/A
0.47	~ 86000	279	5.1	65
0.49	~ 580000	258	5.9	92

Table 4. Comparison of characteristic rheological and density relaxation times for bare and 5% silanized particles in PEG-400.

IV. CONCLUSION

In designing polymer nanocomposites the goal is often to load the system with particles to control composite rheology. Particles are known to increase composite viscosity and increase polymer mechanical relaxation times. Increasing the change in enthalpy that occurs when a segment is transferred from the bulk to the particle surface is known to increase the particle hydrodynamic size and decrease the particle volume fraction where the particles undergo a colloidal glass transition. However, we show here that even for unentangled polymers, when the particles approach a distance of less than $6Rg$, the adsorbed polymer layers interact such that composite rheology is increasingly dominated by the polymer relaxations while for separations greater than $6Rg$ the composite mechanical relaxations are dominated by colloidal properties much the same way as particles suspended in a low molecular weight solvent. Here we have extended these observations to particles that have been designed to lower the strength of segment adhesion to the particle surface.

PEG is expected to hydrogen bond to a bare silica surface such that if the surface is rendered hydrophobic by reactions with butyl silanes, the strength of segment adsorption will decrease. The reaction chemistry undertaken here to render the particles hydrophobic was done under conditions where the silane is known to form monomeric coverage of the surface rather than polymeric siloxane films that might result in a more patchy surface.[32] Silica particles reacted with 0-5% silane by weight of silica formed stable suspensions in PEG400 showing no indications of aggregation from X-ray scattering up to the highest volume fractions probed. With increasing silanization, the structural data shows a non-monotonicity, that when interpreted through the framework of PRISM suggests decreasing polymer-particle interaction strength ε_{pc} , with a subsequent recovery as silanization is increased. Since ε_{pc} is a chemistry specific parameter, and should therefore

be expected to decrease monotonically with increasing surface coverage, the trends suggest that there are other factors such as configurational changes of the adsorbed polymer not captured by PRISM, that may be responsible for non-monotonic trends seen here. For higher volume fractions, the particle microstructure in the composite shows characteristics common to soft systems where the particles in the first nearest neighbor cage de-correlate over a range of volume fractions as indicated by a maximum in $S(q^*D_c)$. Differences consistent with more mobile adsorbed polymer layers in silanized suspensions are seen at volume fractions where $6 > h/Rg$. These differences are associated with a higher volume fraction where $S(q^*D_c)$ reaches a maximum, faster density relaxations, delayed upturn in density relaxations and dramatically reduced low shear rate viscosities for 5% silanized composites.

While the microstructure is sensitive to the degree of silanization, the flow properties of composites of silica and PEG400 are not altered by the degree of silanization up to volume fractions above the colloidal glass transition. Only at volume fractions where adsorbed polymer layers begin to interact strongly ($h/Rg < 6$) does the zero shear rate viscosity decrease dramatically with increased degree of silanization. We note that caging as measured by p values occurs at the same volume fraction for both systems (ϕ_{eff} =0.51, $\phi_c = 0.43$). At larger values of ϕ_c the p values drop rapidly for the bare particles indicating rapidly increasing values of Γ_r. For the silanized particles, over the volume fraction range studied, for $\phi_c > 0.43$, p approaches a plateau value indicating weak dependence of Γ_r on volume fraction even though the particles have apparently entered a glassy state. This behavior is associated with particles reaching average surface separations of $h/Rg \sim 6$ where microstructural studies provide evidence that the particle potential of mean force for both bare and silanized particles changes dramatically.

These results indicate that for the 5% silanized samples, if interpreted with PRISM, polymer segments and the particle surface experience the same enthalpy of adsorption resulting in an adsorbed polymer layer with the same hydrodynamic thickness as the bare particles. The hydrodynamic interactions of particles coated with these layers are not affected by small changes to polymer mobility in these layers until the layers are brought into close contact. For $h/Rg < 6$, we observe that with increasing silanization, particles retain greater mobility, and composite viscosities are dramatically lowered indicating increasing softness with silanization.

Although faster density relaxations are observed for 5% silanized samples compared to bare which is consistent with rheology measurements as characterized by dynamic X-ray scattering, the characteristic relaxation times measured suggest that density fluctuations are not relaxing by diffusive mechanisms and that this mechanism is not correlated with stress relaxation times as characterized by Γ_r.

From these observations we conclude that silanization alters polymer adsorption in a way that enables faster relaxations and softer adsorbed layer interactions. This is supported by our observations that in the regime where the rheological, structure and transport properties are dominated by the characteristics of the adsorbed polymer layer when h/Rg

< 6, we see substantial changes with increasing silanization consistent with increasing softness.

REFERENCES

1. P. M. Ajayan, L. S. Schadler and P. V. Braun, *Nanocomposite Science and Technology*, Wiley-VCH, Weinheim, 2003.
2. A. C. Balazs, T. Emrick and T. P. Russell, *Science*, 2006, **314**, 1107-1110.
3. M. J. Wang, *Rubber Chem Technol*, 1998, **71**, 520-589.
4. J. B. Hooper and K. S. Schweizer, *Macromolecules*, 2005, **38**, 8858-8869.
5. J. B. Hooper and K. S. Schweizer, *Macromolecules*, 2006, **39**, 5133-5142.
6. L. M. Hall, B. J. Anderson, C. F. Zukoski and K. S. Schweizer, *Macromolecules*, 2009, **42**, 8435-8442.
7. S. Y. Kim and C. F. Zukoski, *Soft Matter*, 2012, **8**, 1801-1810.
8. S. K. Kumar, N. Jouault, B. Benicewicz and T. Neely, *Macromolecules*, 2013, **46**, 3199-3214.
9. D. L. Green and J. Mewis, *Langmuir : the ACS journal of surfaces and colloids*, 2006, **22**, 9546-9553.
10. S. Y. Kim and C. F. Zukoski, *Langmuir : the ACS journal of surfaces and colloids*, 2011, **27**, 10455-10463.
11. L. M. Hall and K. S. Schweizer, *Journal of Chemical Physics*, 2008, **128,** 234901.

12.   B. J. Anderson and C. F. Zukoski, *Langmuir : the ACS journal of surfaces and colloids*, 2010, **26**, 8709-8720.
13.   B. J. Anderson and C. F. Zukoski, *Macromolecules*, 2008, **41**, 9326-9334.
14.   S. Y. Kim, H. W. Meyer, K. Saalwachter and C. F. Zukoski, *Macromolecules*, 2012, **45**, 4225-4237.
15.   S. Y. Kim, K. S. Schweizer and C. F. Zukoski, *Physical Review Letters*, 2011, **107**, 225504.
16.   B. J. Anderson and C. F. Zukoski, *Journal of Physics-Condensed Matter*, 2009, **21**, 285102.
17.   B. J. Anderson and C. F. Zukoski, *Macromolecules*, 2009, **42**, 8370-8384.
18.   L. Berthier, A. J. Moreno and G. Szamel, *Physical Review E*, 2010, **82**, 060501.
19.   S. Srivastava, L. A. Archer and S. Narayanan, *Physical Review Letters*, 2013, **110**, 148302.
20.   A. Madsen, R. L. Leheny, H. Y. Guo, M. Sprung and O. Czakkel, *New J Phys*, 2010, **12**, 055001.
21.   P. N. Pusey and R. J. A. Tough, *Dynamic Light Scattering*, Plenum Press, New York, 1985.
22.   L. Cipelletti, S. Manley, R. C. Ball and D. A. Weitz, *Physical Review Letters*, 2000, **84**, 2275-2278.
23.   L. Cipelletti, L. Ramos, S. Manley, E. Pitard, D. A. Weitz, E. E. Pashkovski and M. Johansson, *Faraday Discuss*, 2003, **123**, 423-423.
24.   H. Guo, J. N. Wilking, D. Liang, T. G. Mason, J. L. Harden and R. L. Leheny, *Physical Review E*, 2007, **75**, 041401.
25.   H. Y. Guo, G. Bourret, M. K. Corbierre, S. Rucareanu, R. B. Lennox, K. Laaziri, L. Piche, M. Sutton, J. L. Harden and R. L. Leheny, *Physical Review Letters*, 2009, **102**, 075702.
26.   H. Y. Guo, S. Ramakrishnan, J. L. Harden and R. L. Leheny, *Journal of Chemical Physics*, 2011, **135**, 154903.
27.   L. Ramos and L. Cipelletti, *Physical Review Letters*, 2001, **87**, 245503.
28.   G. Das, N. Gnan, F. Sciortino and E. Zaccarelli, *Journal of Chemical Physics*, 2013, **138**, 134501.
29.   J. R. Errington and P. G. Debenedetti, *Nature*, 2001, **409**, 318-321.
30.   K. R. Harris and L. A. Woolf, *J Chem Soc Farad T 1*, 1980, **76**, 377-385.
31.   A. Scala, F. W. Starr, E. La Nave, F. Sciortino and H. E. Stanley, *Nature*, 2000, **406**, 166-169.
32.   E. P. Plueddemann, *Silane Coupling Agents*, Plenum Press, New York, 1991.
33.   W. Stober, A. Fink and E. Bohn, *J Colloid Interf Sci*, 1968, **26**, 62-69.
34.   G. H. Bogush, M. A. Tracy and C. F. Zukoski, *J Non-Cryst Solids*, 1988, **104**, 95-106.
35.   J. H. Moon, J. W. Shin, S. Y. Kim and J. W. Park, *Langmuir : the ACS journal of surfaces and colloids*, 1996, **12**, 4621-4624.
36.   J. Mewis and N. J. Wagner, *Colloidal Suspension Rheology*, Cambridge University Press, New York, 2012.
37.   T. Y. Jiang and C. F. Zukoski, *Macromolecules*, 2012, **45**, 9791-9803.
38.   Z. D. Cheng, J. X. Zhu, P. M. Chaikin, S. E. Phan and W. B. Russel, *Physical Review E*, 2002, **65**, 041405.

39.   D. M. Heyes and A. C. Branka, *Journal of Chemical Physics*, 2005, **122**, 234504.
40.   D. M. Heyes and A. C. Branka, *Journal of Physics-Condensed Matter*, 2008, **20**, 115102.
41.   T. Y. Jiang and C. F. Zukoski, *Soft Matter*, 2013, **9**, 3117-3130.
42.   M. J. Pond, J. R. Errington and T. M. Truskett, *Journal of Chemical Physics*, 2011, **134**, 081101.
43.   M. J. Pond, J. R. Errington and T. M. Truskett, *Soft Matter*, 2011, **7**, 9859-9862.
44.   F. Saija, S. Prestipino and G. Malescio, *Physical Review E*, 2009, **80**, 031502.
45.   M. Watzlawek, H. Lowen and C. N. Likos, *Journal of Physics-Condensed Matter*, 1998, **10**, 8189-8205.
46.   S. Granick and H. W. Hu, *Langmuir : the ACS journal of surfaces and colloids*, 1994, **10**, 3857-3866.
47.   H. W. Hu and S. Granick, *Science*, 1992, **258**, 1339-1342.
48.   B. Chung, S. Ramakrishnan, R. Bandyopadhyay, D. Liang, C. F. Zukoski, J. L. Harden and R. L. Leheny, *Physical Review Letters*, 2006, **96**, 228301.
49.   E. M. Herzig, A. Robert, D. D. van't Zand, L. Cipelletti, P. N. Pusey and P. S. Clegg, *Physical Review E*, 2009, **79**, 011405.
50.   K. Laszlo, A. Fluerasu, A. Moussaid and E. Geissler, *Soft Matter*, 2010, **6**, 4335-4338.
51.   A. Robert, E. Wandersman, E. Dubois, V. Dupuis and R. Perzynski, *Europhys Lett*, 2006, **75**, 764-770.
52.   C. Caronna, Y. Chushkin, A. Madsen and A. Cupane, *Physical Review Letters*, 2008, **100**, 055702.
53.   A. Duri, T. Autenrieth, L. M. Stadler, O. Leupold, Y. Chushkin, G. Grubel and C. Gutt, *Physical Review Letters*, 2009, **102**, 145701.
54.   S. Schramm, T. Blochowicz, E. Gouirand, R. Wipf, B. Stuhn and Y. Chushkin, *Journal of Chemical Physics*, 2010, **132**, 224505.